Data Folding for the LIGO Stochastic Directional Analysis Pipeline

Eli Wiston
University of Pennsylvania

Mentors: Arianna Renzini and Colm Talbot
California Institute of Technology
(Dated: October 29, 2021)

While a growing number of individual gravitational wave events have been observed, researchers are still searching for a stochastic gravitational-wave background. This superposition of weak, unresolved gravitational-wave signals could hold a wealth of both astrophysical and cosmological information. Studying both the isotropic and anisotropic components of the background at current detector sensitives could provide a measure of matter distributions and large-scale structure in the Universe. Eventually these searches may provide concrete evidence of inflation and act as a primordial analog to the Cosmic Microwave Background. This paper will detail the development of a data folding algorithm for the stochastic gravitational wave background analysis pipeline. Taking advantage of the fact that the detector response is periodic with the rotation of the Earth, long stretches of time series data can be condensed to the size of one sidereal day. We implement this algorithm in both simulated and real data and verify it's efficacy through direct comparison to calculations with unfolded data. With the implementation of data folding, anisotropic directional searches can be carried out far more efficiently. Data folding only needs to be applied once, but brings orders of magnitude improvements in speed and data size, with negligible loss of information.

I. INTRODUCTION

In 2015, LIGO made the first direct detection of a gravitational wave (GW) signal [1]. Since then, interferometers have measured many more signals from black hole and neutron star binaries [2]. These binaries must either have very high mass or be very compact in order to be detected by current ground-based detectors. However, the sky is filled with gravitational wave signals below detection thresholds that, when analyzed as a whole, contain a great deal of information. These signals are unresolved, numerous, and best described according to probability distributions, hence they are known as the stochastic gravitational wave background (SGWB) [3].

SGWB searches can be performed as either all-sky or directional searches. Isotropic searches model the background with no directional dependence and can be used to characterize the average GW signal in the Universe. Directional searches account for potential variation across the sky and can be used to map anisotropies in the GW distribution [3]. Due to the Earth's rotation, ground-based detectors measure the signal on the sky in a time-dependent manner, which is periodic over a sidereal day.

This project is focused on developing a key component of LIGO's SGWB pipeline: data folding. Because LIGO data is periodic over one day, we can compress the time series information we measure. By folding gravitational wave data over one sidereal day, the efficiency of current and future directional stochastic searches can be vastly improved.

The contents of this report will be presented as follows. In Section II, we present a brief overview of the motivations for stochastic gravitational wave searches. In Section III, we provide the necessary background, starting with gravitational waves in general and then going over stochastic signals and their measurement and analysis. Section IV details the data folding approach, modeled after the work in [4]. In Section V, the algorithm is applied to a simulated dataset and in Section VI, it is applied to real LIGO data. In Section VII, we present our conclusions and next steps, and Section VIII features acknowledgments.

II. MOTIVATIONS

Gravitational waves provide one way for researchers to probe the Universe without relying on extraterrestrial electromagnetic signals. This can be incredibly useful, providing independent measurements of electromagnetic sources and new measurements of GW sources. High signal-to-noise measurements can provide insight into individual events, but the stochastic gravitational wave background can provide information about large scale structure and cosmology [5].

The earliest electromagnetic signals come from the time of last scattering, at a redshift of around $z = 1100$, and comprise the Cosmic Microwave Background (CMB) [6]. Before then, the Universe was too opaque for photons to travel very far. However, gravitational waves were able to propagate all the way back in the early moments of the Universe. Eventually, stochastic gravitational wave searches may be able to find direct evidence of inflation and provide information about potential early Universe phase transitions [7].

Current detectors lack the sensitivity to measure the comparatively weak signals from these cosmological background events, but they can be used to study sources which lie at astrophysical redshifts. These sources are

expected to be distributed somewhat anisotropically. A directional search looking at these anisotropies in the SGWB can probe at the Universe's underlying mass distribution. In particular, these searches can provide strong tests of the expected distribution of compact binary coalescences (CBCs)[8].

III. BACKGROUND

A. Gravitational Waves

Gravitational waves manifest as strains in the spacetime metric. They arise when the quadrapole mass moments of objects, I_{uv} have a time dependence [9]. This is why the direct detections already made involve compact objects inspiraling. In the context of general relativity, gravitational waves can be thought of as linear perturbations of the background metric g_{uv}. Assuming that the gravitational field is weak and non-stationary, one can show that the solution to the Einstein field equations for such a perturbation can be constructed as a plane wave, propagating at the speed of light [10].

Currently, the primary method for detecting gravitational waves is ground-based interferometry. The basic setup is that of a Michelson interferometer. A laser beam is split along two long, perpendicular arms and reflected off of mirrors, combining again at a photodetector. Gravitational waves strain the travel distance along the arms, creating an optical phase difference between the two beams. With a new phase difference, the electromagnetic laser waves interfere slightly differently, manifesting in a change in light intensity at the frequency of the wave, which one can directly measure. From these measurements, one may be able to determine the frequency, amplitude, direction, and polarization of the wave. Gravitational wave strains are incredibly small, so interferometers have to be extremely sensitive to detect them. At peak sensitivity in the O3 observing run, the displacement sensitivity was on the order 10^{-20} meters [11]. There are many sources of noise that also make detection difficult, including seismic activity and Brownian motion of the detector mirrors [9].

B. Stochastic Signals

Due to the low signal-to-noise nature of gravitational waves, only the most extreme GW events can be directly detected. However, these types of events constitute a tiny fraction of all gravitational wave signals; the rest comprise the stochastic gravitational wave background. These stochastic signals are weak, independent, random, and unresolved. The distinction between a stochastic and resolvable signal can be unclear, as it may depend on modelling decisions or the precision of a detector. A signal can be operationally defined as stochastic if a Bayesian model selection calculation prefers a stochastic signal model over any deterministic signal model [3]. There are two broad categories of stochastic GW signals, based on the nature of the GW source: astrophysical and cosmological. Astrophysical signals occur at low redshift and are stochastic in the limit that number of sources N is very high. They are mainly comprised of compact binary systems. Cosmological signals arise from processes in the early Universe. They can be described stochastically as a result of the assumed homogeneity and isotropy of the universe. All inflationary models have some gravitational wave byproducts. Early universe phase transitions are also predicted to produce detectable signals [7]. LIGO does not currently have the sensitivity to measure weak cosmological signals, so this analysis will be aimed at measuring the astrophysical foreground.

A key parameter of interest in SGWB searches is Ω_{gw}, the fractional energy density of gravitational waves in the universe. In general, the parameter will be a function of both frequency and direction, expressed as $\Omega_{gw}(f, \hat{n})$ [3]. Searches performed on LIGO's first three runs have not detected a stochastic background, but have set upper limits on Ω_{gw}. These limits fall in line with predictions based on the expected distribution of compact binary systems [8, 12].

C. Measurement and Analysis

The stochastic signal h_{ab} can be expressed as a superposition of sine waves as follows:

$$h_{ab}(t, \vec{x}) = \int_{-\infty}^{+\infty} df \int d^2\Omega_{\hat{n}} h_{ab}(f, \hat{n}) e^{i2\pi f(t+\hat{n}\cdot\vec{x}/c)} \quad (1)$$

where $h_{ab}(f, \hat{n})$ are the random variable Fourier coefficients that can be used to statistically describe the background. We can assume the background has zero mean, so $< h_{ab} >= 0$. For Gaussian sources, the signal is therefore entirely characterized by its second order moment. These quadratic expectation values can be defined in terms of the strain density power spectrum $\mathcal{P}_h$. According to [3]:

$$< h_A(f, \hat{n}) h^*_{A'}(f', \hat{n'}) >= \frac{1}{4}\mathcal{P}_h(f, \hat{n})\delta(f-f')\delta_{AA'}\delta^2(\hat{n}, \hat{n'}) \quad (2)$$

From $\mathcal{P}_h$, $\Omega_{gw}(f, \hat{n})$ can be found through a simple relation:

$$\mathcal{P}_h(f, \hat{n}) = \frac{3H_0^2}{8\pi^3}\frac{\Omega_{gw}(f, \hat{n})}{f^3} \quad (3)$$

The signal-to-noise of the stochastic background is far too low to extract any meaningful information from a single detector. However, by cross-correlating the strain data between multiple detectors, the stochastic signal can be found. The detectors will be measuring the same true signal, so those will add coherently. The noise in each

detector, on the other hand, is independent and will not add coherently. Given a Gaussian approximation, the noise will be averaged down as $1/\sqrt{\text{time}}$, while the signal will remain unsuppressed. The signal cross-correlation, discussed in detail in Section IV, is directly related to key parameters, including $\mathcal{P}_h$. By performing maximum likelihood analyses, one can calculate $\mathcal{P}_h$ from the observed cross-correlated data [3].

The longer the observation time being analyzed, the more the noise is suppressed. However, dealing with long periods of time is computationally demanding, both in terms of processing power and storage. This issue can be confronted by folding the strain data. We fold over one sidereal day so anisotropies in the same region of the sky can add coherently. Ain, Dalvi, and Mitra developed the algebra and algorithm for such data folding [4]. Testing on LIGO S5 data, they found very significant decreases in computation time. An analysis of the full S5 data on folded data was faster than the same analysis of unfolded data by a factor of 300. Furthermore, the data quality was virtually unchanged; the differences between folded and unfolded maps were orders of magnitude smaller than the values themselves. The folding increases efficiency, portability, and convenience, facilitating more analyses of strain data, carried out at faster rates.

IV. APPROACH

The overall goal of a directional search is to estimate the amplitude of the SGWB power spectral density (PSD) as a function of position in the sky. For current searches, the shape of the PSD as a function of frequency is assumed. This assumption will work well for this project, since the PSD shape for the CBC dominated background is well known.

The time series data from a each detector, $s(t)$ is the sum of the stochastic signal and detector noise. Following the approach in [4], it is convenient to divide the data for each baseline $\mathcal{I}$ into short time segments of length τ. A Fourier transform is then performed on each of these segments as follows:

$$\tilde{s}_{\mathcal{I}}(t;f) = \int_{t-\tau/2}^{t+\tau/2} dt' s(t') e^{-i2\pi f t'} \tag{4}$$

The maximum likelihood solution for the coefficients of the SGWB skymap, $\hat{P}$ can be calculated using two matrix quantities, the dirty map X and the Fisher information matrix Γ [3]:

$$\hat{P} = \Gamma^{-1} \cdot X \tag{5}$$

where,

$$X = \frac{4}{\tau} \sum_{Ift} \frac{H(f)\gamma^*_{ft,\alpha}}{P_{I_1}(t;f)P_{I_2}(t;f)} S_{I_1,I_2}(t;f) \tag{6}$$

$$\Gamma = 4 \sum_{Ift} \frac{H^2(f)}{P_{I_1}(t;f)P_{I_2}(t;f)} \gamma^{I*}_{ft,\alpha}\gamma^{I}_{ft,\alpha'} \tag{7}$$

$H(f)$ is the expected shape of the stochastic background's frequency power spectral density (see subsection A). $P_{I_{1,2}}$ is the one-sided power spectral density of the noise for a segment of time and S_{I_1,I_2} is the cross correlated power between both detectors (see subsection B). $\gamma^{I*}_{ft,\alpha}$ is the overlap function, containing all the specific information about the detectors' antenna pattern functions, baseline separations, and polarization (see subsection C).

A. Expected Frequency Distribution

We assume that the SGWB is stationary, i.e., not evolving in time. This assumption holds in the low redshift, astrophysical regime, provided there are a large number of sub-threshold compact binaries. The high redshift, cosmological regime is a primordial signal that permeates the universe and is stationary much in the same way the CMB is stationary. Therefore our assumed shape of the SGWB is only dependent on frequency.

The assumed frequency distribution is predicted by several theoretical models to follow a power law:

$$H(f) = A_\beta \Big(\frac{f}{f_{\text{ref}}}\Big)^\beta \tag{8}$$

For a CBC dominated background $\beta = -7/3$; however, for the purposes of testing in this paper, we'll use a simple flat distribution with $\beta = 0$:

$$H(f) = 1 \tag{9}$$

B. Power Spectral Density and Cross Spectral Density

The PSDs, or autocorrelations, are calculated by convolving the Fourier transformed data from a given detector with itself:

$$P_{1,2} = \tilde{s}_{\mathcal{I}_1}(t;f)\tilde{s}^*_{\mathcal{I}_1}(t;f). \tag{10}$$

The PSDs are a measure of the dectector noise at different frequencies.

The CSD, or cross power, is calculated by convolving the data from two different detectors:

$$S_{12} = \tilde{s}_{\mathcal{I}_1}(t;f)\tilde{s}^*_{\mathcal{I}_2}(t;f). \tag{11}$$

The key to detecting low signal-to-noise stochastic signals lies in this cross correlation. While a pair of detectors will receive the same signal, their noise should be completely uncorrelated. When the data from each detector is cross correlated, the signal will add coherently, while the noise (assuming Gaussianity) will average down

by $1/\sqrt{N_{\text{segments}}}$, where N_{segments} is the number of short time segments being averaged over.

For a demonstration of this effect, colored Gaussian time series data was generated based on the LIGO design sensitivities for the Livingston and Hanford detectors. A very loud, coherent signal was then injected into both detectors centered at 200 Hz. In order to visualize the effect of cross correlation, we look at the coherence, which is equal to the CSD normalized by both corresponding detector PSDs:

$$C_{12} = \frac{S_{12}}{\sqrt{P_1 P_2}} \tag{12}$$

In Figure 1, we plot the coherence of this signal is plotted as a function of time. We see that the coherence is equal to 1 around 200 Hz where the signal was injected. At the other frequencies, the coherence has been averaged down by the expected factor of $1/\sqrt{N_{\text{segments}}}$.

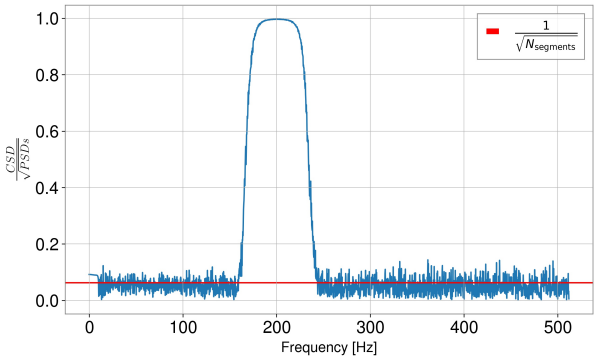

FIG. 1. Plot of coherence as a function of frequency for an injected signal centered at 200 Hz. At all other frequencies, the data are uncorrelated between the two simulated detectors, resulting in a coherence of $1/\sqrt{N_{\text{segments}}}$. For this idealized case, the injected signal is perfectly coherent between the detectors

C. Overlap Function

The overlap function γ describes the relationship between the power of the SGWB and the cross-correlated response of a baseline of two detectors [13]. Essentially, it is a measure of the baseline's sensitivity to different parts of the sky, which varies as a function of frequency and time. The function is given by:

$$\gamma^I_{ft} = \sum_A F^A_{\mathcal{I}_1}(d\hat{\Omega}, t) F^A_{\mathcal{I}_2}(d\hat{\Omega}, t) e^{2\pi i f \frac{\hat{\Omega}\Delta x_I(t)}{c}} \tag{13}$$

where $F^A_{\mathcal{I}_{1,2}}$ is the antenna pattern function of the two detectors, A is the polarization, and Δx is the separation between the detectors.

In Figure 2, the overlap function is visualized by skymaps at different moments in time. As seen in the figure, the function has two large areas of maximum sensitivity and a band of minimum sensitivity separating them. Over the course of the day, the overlap function rotates along with the rotation of the Earth, completing one rotation each sidereal day. If the sensitivity is periodic over one sidereal day and the SGWB is relatively stationary, the response from each baseline should also be periodic each day.

Alternatively, the overlap function can be visualized in 3D space, as in Figure 3. In these plots, the sky is represented as a 3D surface and the magnitude of the sensitivity is represented by the radius at each point. In this visualization, the two strong responses are seen most clearly.

There exists an optimal basis in which to visualize the periodicity of the overlap function. The spherical harmonic functions, Y^l_m, form a complete, orthonormal basis and, therefore, any function defined on the surface of a sphere can be re-written as a summation. For the overlap function:

$$\gamma(\theta, \phi) = \sum_{l,m} \gamma_{lm} Y^l_m(\theta, \phi) \tag{14}$$

The order of the harmonic l denotes the moment (monopole, dipole, etc.). The specific mode m corresponds to the frequency of oscillations. Each moment l has modes ranging from -l to +l. Each (l,m) mode can be found by integrating the overlap function multiplied by the spherical harmonic over the sky.

$$\gamma_{lm} = \int d\Omega \gamma(\theta, \phi) Y^{l*}_m(\theta, \phi) \tag{15}$$

In Figure 4, this transformation is applied to the first 3 moments of the overlap function. As expected, the monopole term is constant in time. Due to the azimuthal symmetry of the system, all 3 dipole terms are equal to 0. The quadrupole terms illustrate how the mode number m corresponds to the frequency of oscillations. The $m = 0$ term is constant in time. The $m = -1, +1$ terms go through one period over the course of a day, while the $m = -2, +2$ terms go through two periods. A factor of $(-1)^m$ accounts for the reflection in the $-1, +1$ modes.

The power spectra for the overlap can be calculated by summing over all the m modes in the following equation:

$$\Gamma_l = \frac{1}{2l+1} \sum_m |\gamma_{lm}|^2 \tag{16}$$

The power for each moment at fixed time is shown in Figure 5. Here we see that the azimuthal symmetry ensures that all odd moments drop to 0, verifying that the overlap function is even.

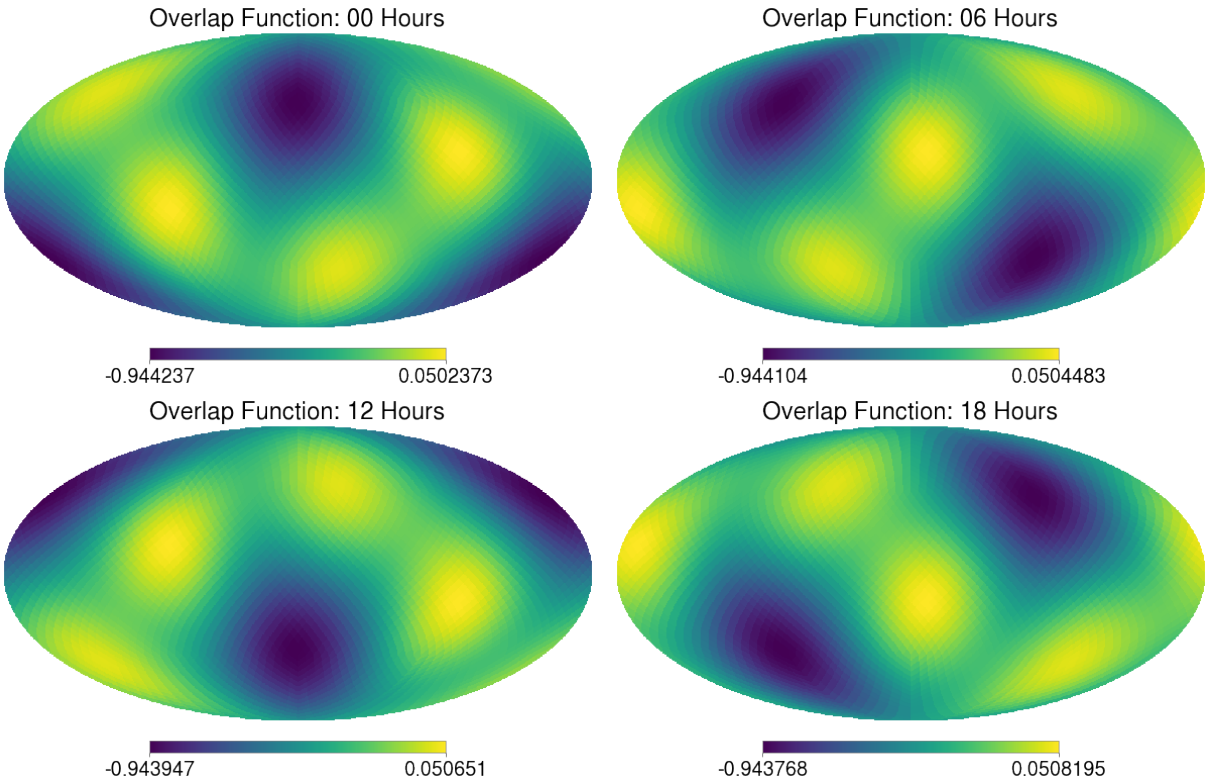

FIG. 2. The time-evolved overlap function for the baseline of the LIGO Hanford and LIGO Livingston detectors. As the Earth rotates, the sensitivity pattern rotates with it, in a way that is periodic over one sidereal day.

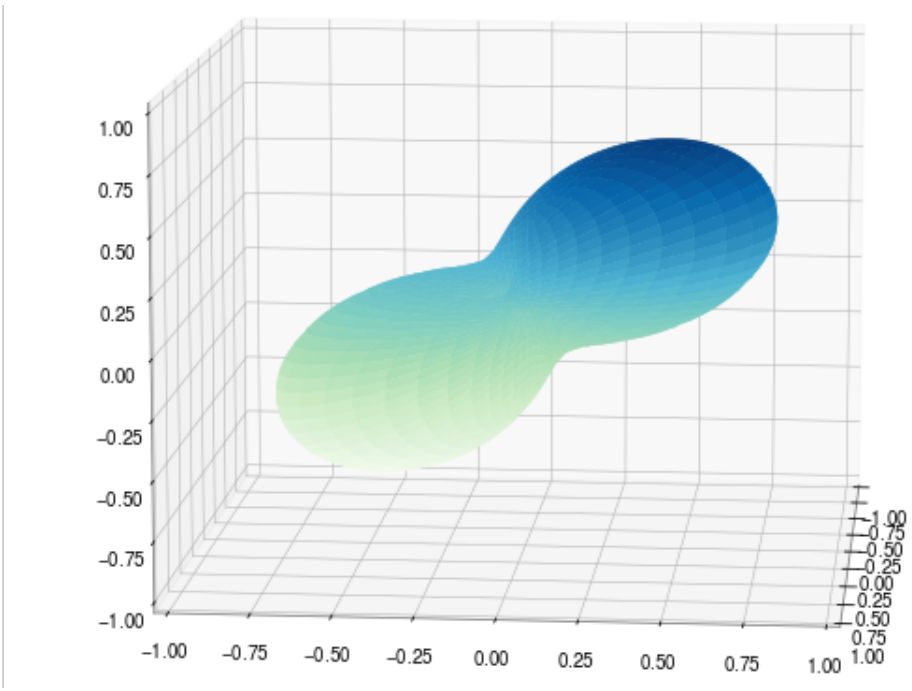

FIG. 3. Alternate visualization of the overlap function. The value of the function at any given point corresponds to the radius. In this visualization, the two strong responses across the sky are made very apparent.

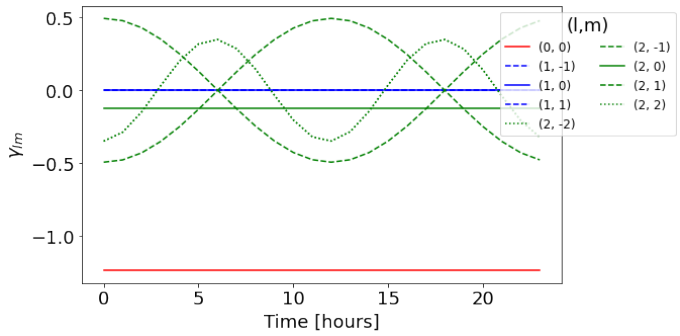

FIG. 4. First 3 γ_{lm} moments as a function of time. Monopole terms are shown in red, dipole in blue, and quadrupole in green. Crucially, each function is periodic over one sidereal day.

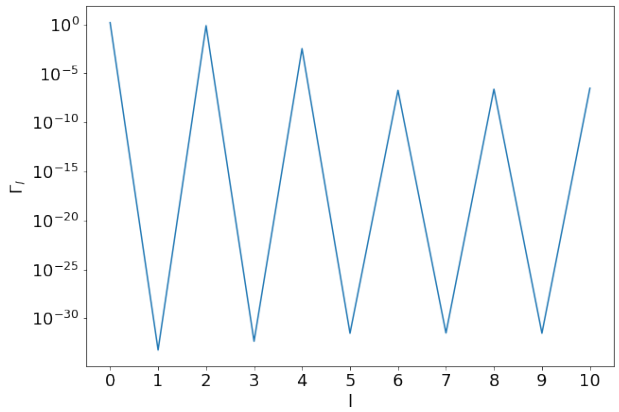

FIG. 5. Γ_l for the first 10 moments of the overlap function. The function is entirely even, with all the odd moments dropping to 0.

D. Folding

Taking advantage of the fact that $H(f)$ is not time dependent and γ is periodic over a day, (6) can be broken into two summations:

$$X = \frac{4}{\tau}\sum_{Ift_s} H(f)\gamma^{I*}_{ft_s}\sum_{i_{\rm day}}\frac{S_{12}(i_{\rm day}T_s + t_s; f)}{P_{1,2}(i_{\rm day}T_s + t_s; f)}, \quad (17)$$

$$\Gamma = 4\sum_{Ift_s} H^2(f)\gamma^{I*}_{ft_s}\gamma^{I}_{ft_s}\sum_{i_{\rm day}}\frac{1}{P_{1,2}(i_{\rm day}T_s + t_s; f)}, \quad (18)$$

where T_s is the length of a sidereal day and t_s is the time from the start of each day,

$$S_{12} = \tilde{s}_{\mathcal{I}_1}(i_{\rm day}T_s + t_s; f)\tilde{s}^*_{\mathcal{I}_2}(i_{\rm day}T_s + t_s; f), \quad (19)$$

and

$$P_{1,2} = P_{I_1}(i_{\rm day}T_s + t_s; f)P_{I_2}(i_{\rm day}T_s + t_s; f) \quad (20)$$

Performing the summation over i_{day} folds the data, with the information from months or years compressed into one sidereal day. This summation only needs to be performed once, but all subsequent analysis on folded data will be sped up by a factor of N_{days}.This process is shown below in Figure 6, visualized by [4]. The corresponding times at each point of the sidereal day (the top three circles) are averaged together to produce one day's worth of data (the bottom circle).

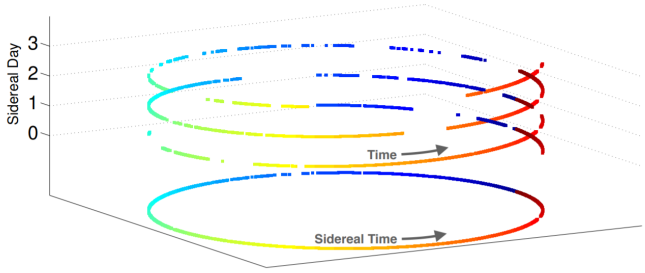

FIG. 6. Folding process visualized for 3 days of LIGO S5 data. The three top rings are projected onto the ring below, representing the folding data. Gaps in the rings represent missing data. [4]

E. Mitigating Information Loss in Folding

Calculating the CSD and PSDs involves some choice of fast Fourier transform segment duration, τ. This presents a possible issue when trying to fold the data. Ideally, the time segments would fit neatly into one sidereal day and every segment could be averaged together with the corresponding segments in every other day. However, a primary goal of this folding code is to allow for flexible use, including any choice of segment duration. Using a duration that isn't a factor of one day inherently comes with a loss of information.

We consider two methods to deal with this duration problem: cutting days down to be divisible by the given duration or lining times in each day up as close as possible, accepting that segments will be slightly offset from one another. The information loss from these two different methods at various segment lengths can be directly computed. The loss from the cutting method can be simply calculated as the percentage of data being cut.

$$\text{loss}_{\rm cut} = \frac{(t_{\rm day} \bmod t_{\rm segment})}{t_{\rm day}} \quad (21)$$

The loss from two segments being offset can be calculated by comparing the convolution of the overlap function at different offsets to the magnitude of the overlap. Assuming that for large total times, the magnitude of the offset between segments is evenly distributed over the range of

possible values $[0, \frac{\tau}{2})$, the total information loss is calculated as:

$$\text{loss}_{\text{offset}} = \int_0^{\frac{\tau}{2}} d(\Delta t) \frac{\sum_{\hat{n}} \gamma(t_0)\gamma^*(t_0 + \Delta t)}{\sum_{\hat{n}} \gamma(t_0)\gamma^*(t_0)} \tag{22}$$

In Figure 7, we see these two methods directly compared. The information loss for the cutting method (blue) and the offset method (orange) are plotted as a function of segment duration. As seen in the figure, the offset method consistently performed better than the cutting method, so we implemented this technique in the folding code. The no loss condition (green) is when the segment duration fits evenly into a sidereal day. In the figure, we also see that the longest duration for no loss is only 52 seconds. Such a short duration is not desirable for many analyses, which is why the no loss condition is not always chosen.

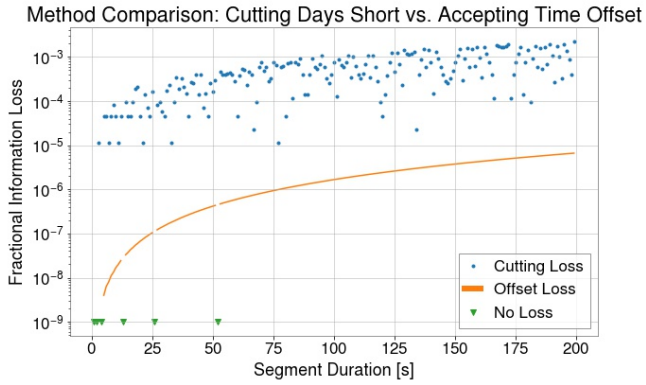

FIG. 7. Comparison of information loss between two methods of handling different segment durations. The no loss points represent durations that fit evenly into one sidereal day. Across all other reasonable segment choices, it appears accepting the time offset will minimize information loss.

F. Folding Algorithm

The workflow for the folding algorithm is visualized in Figure 8. We take as inputs the desired start and end of the time being folded, the interferometers whose data we are using, and the desired fast Fourier transform length. First, we check to see which time segments have valid data in both detectors, by checking which times have the "ANALYSIS-READY" flag. Then, we take those segments and access the data for the time series associated with them. Next, we calculate the CSD and PSDs for those time series, using standard functions in the gwpy python module. Then, we perform our data quality cuts, described in more detail in Section V.

For a given Fourier transform segment, we cannot use the same data for calculating both the CSD and PSDs. Instead, we estimate the PSD for each segment by averaging the PSDs from the two surrounding segments. Once this is done, we have our calculated spectrograms, which can then be averaged into our final folded spectrograms.

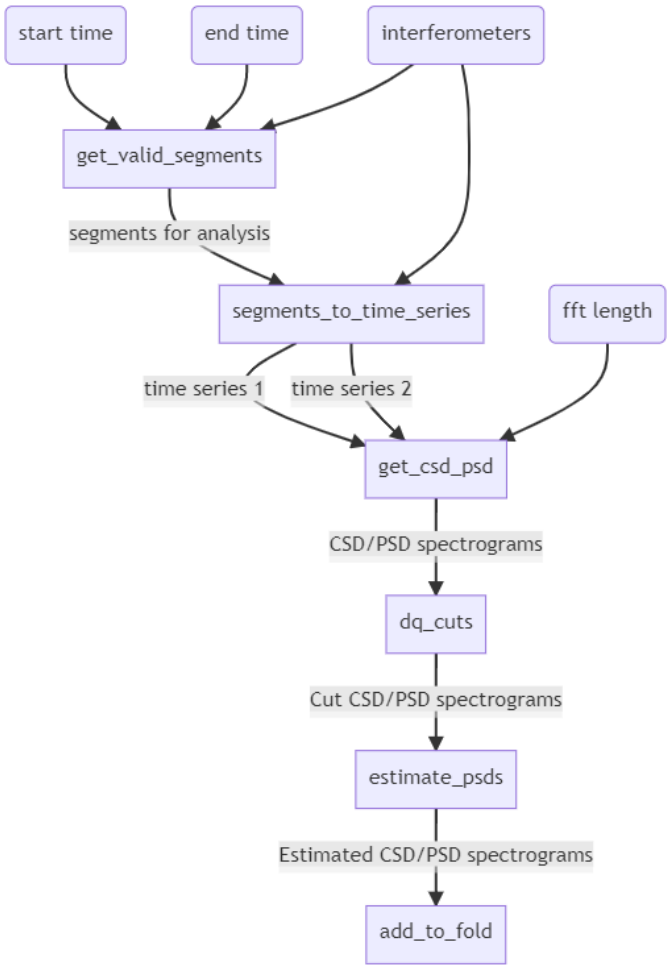

FIG. 8. Workflow for the data folding algorithm. Inputs are the start and end times, interferometers, and fft length and the final output is two folded spectrograms of the terms needed to calculate the dirty map and Fisher matrix.

V. APPLICATION TO SIMULATED DATA

The folding algorithm was first tested on a week's worth of simulated stochastic signal. The simulated dataset included standard colored detector noise, along with an injected high amplitude dipole. In Figure 9, we plot the cross power between the detectors for the full week. We see two strong responses each day, corresponding to detection of both parts of the dipole.

Applying the folding code, the week's worth of data was reduced to the size of one sidereal day. In Figure 10, we plot the folded cross power over one sidereal day. The important features, the two strong responses of the dipole, are left intact.

In order to test whether the folded data is suitable for

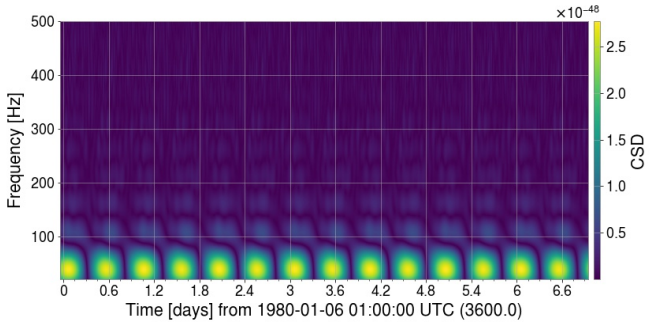

FIG. 9. Cross power for one week's worth of a simulated stochastic dipole.

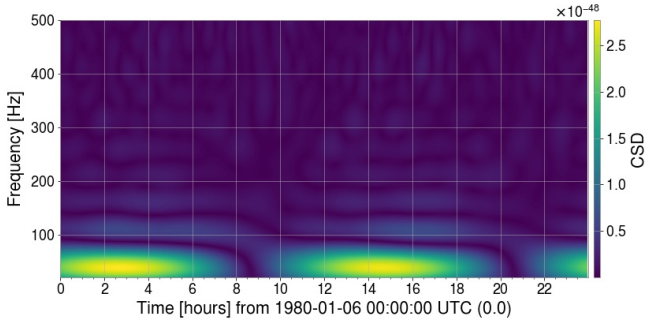

FIG. 10. Stochastic dipole signal cross power folded down to the size of one sidereal day. The coherent signal of the dipole is maintained after the folding process.

analysis, we directly compare the dirty maps produced by Equations (6) and (17), using the unfolded and folded datasets respectively. To assess whether there were significant differences between the maps, the normalized difference was calculated as:

$$\Delta X = \frac{|X_{\text{unfold}} - X_{\text{fold}}|}{\sqrt{X_{\text{unfold}} X_{\text{fold}}}} \tag{23}$$

The results are visualized in Figure 11. Differences between the two maps are relatively small, aside from a few high difference pixels (at around 10%). These can be attributed to numerical errors, rather than any significant information loss in the folding process.

VI. APPLICATION TO LIGO DATA

The folding algorithm was next implemented on real LIGO data, in particular the first half of the O3 run. This data is presented as time-domain strain data over 183 days. While stochastic calculations can involve an arbitrary number of detector baselines, these tests focused on just the Hanford-Livingston baseline.

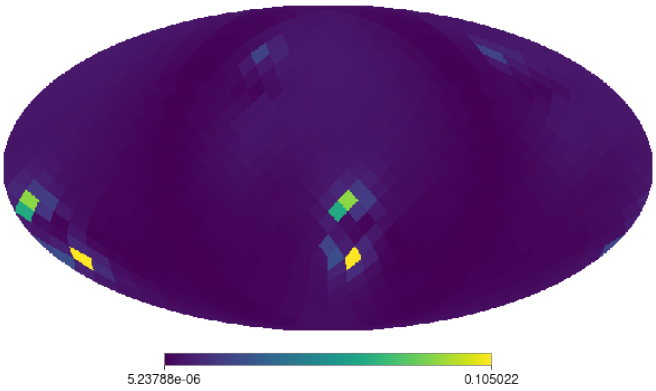

FIG. 11. Normalized difference between unfolded and folded dirty maps, using Equation (23).

A. Data Cuts

Firstly, the time-series data was cut based on when the detectors were actively taking analysis ready data. Both detectors had to be active at a given in order for it to be included. Next, a cut on non-stationary detector noise was implemented via the $\Delta\sigma$ cut. Sigma is defined at each time segment as:

$$\sigma = \sqrt{\sum_f \left(H(f) P_1 P_2 \right)} \tag{24}$$

Using the simplifying assumption of a flat frequency distribution (9), (24) reduces to:

$$\sigma = \sqrt{\sum_f (P_1 P_2)} \tag{25}$$

This value scales with the detector PSDs, and therefore acts as a measure of the noise levels in the detectors. σ values were calculated for each active time segment. For each continuous series of time segments, a median σ value was calculated. σ values within that series that varied by more than 20% from the median were cut (see Figure 12).

The total cuts for all of O3a are visualized in Figure 13. We see two clear distributions: a large, low σ population and a smaller, high σ population. The overlapping region is reflective of the fact that this is not a cut on just high σ, but rather on non-stationary high σ. In total, 28.4% of the data was cut by this process.

The non-stationarity of the detector noise is best seen in Figure 14, whichs plots the median sigma for each day of O3a as a function of time. A baseline σ of around 0.3×10^{-41} seems to be present, but there are many days where noise levels are significantly higher.

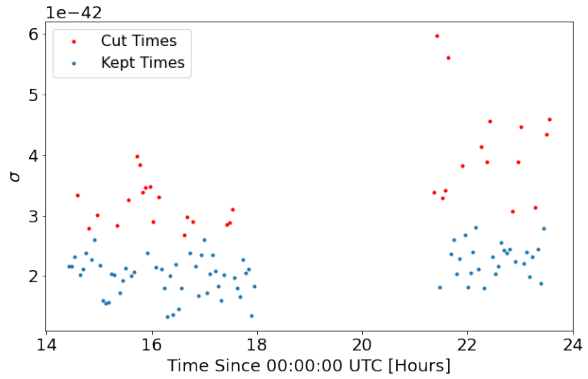

FIG. 12. Delta σ cuts for one sample day in O3a. Non-stationary high σ values are cut from the calculation.

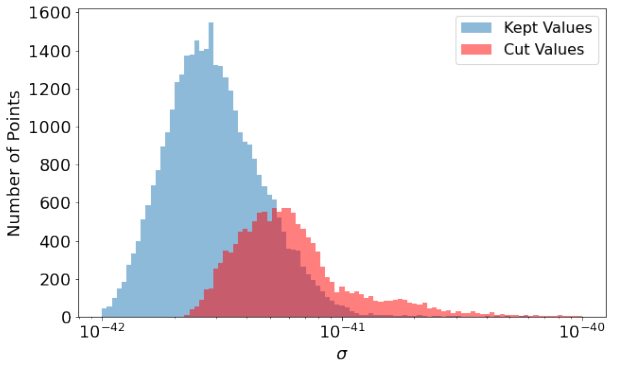

FIG. 13. Histogram of all σ values for the entire O3a dataset. The high σ population in red and the low σ population in blue overlap due to non-stationarity in the detector noise.

B. Results

Performing the folding process on the full O3a dataset, we end up with two final spectrograms: one for the term in the dirty map equation (17) and one for the term in the Fisher matrix equation (18). Both spectrograms are visualized in Figure 15. In the two spectrograms, we observe that there are noise artifacts at characteristic frequencies, producing clear lines in the distribution. In particular, we clearly see the 60 Hz "power line" due to seismic noise and the 300 Hz "violin mode" [14].

Using the folded term in (17), a dirty map was also computed for O3a. The calculated map is shown in Figure 16. The dirty map seems to be consistent with noise levels. Given PSDs at of order 10^{-22}, an amplitude of order 10^{45} is expected.

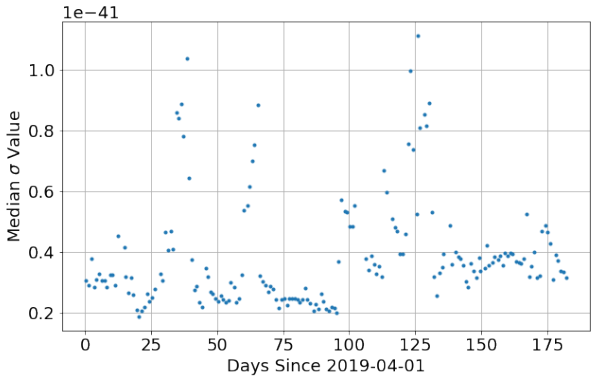

FIG. 14. Median σ values for each day of O3a. This value varies considerably from day to day, changing the standard for which σ values are cut.

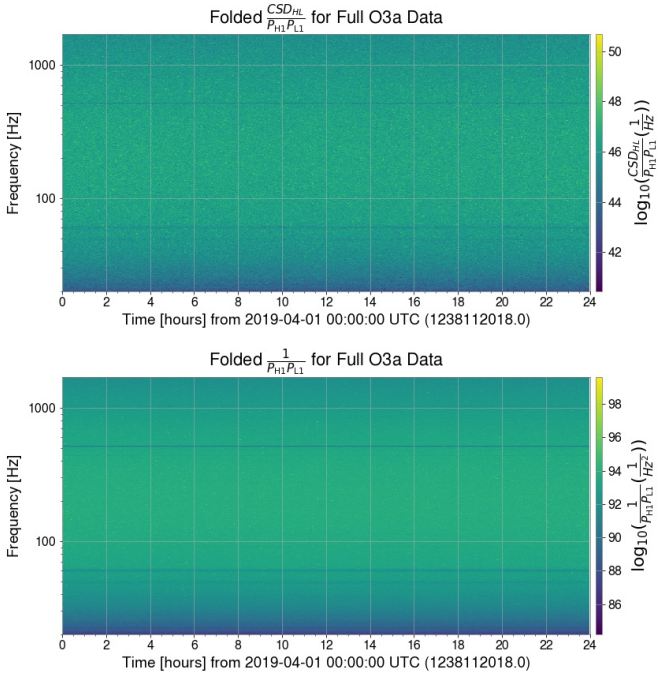

FIG. 15. Final folded spectrograms for the terms necessary to calculate the dirty map and the Fisher information matrix.

VII. CONCLUSIONS AND NEXT STEPS

Stochastic gravitational wave analysis has the potential to provide a wide range of both astrophysical and cosmological insights. In order to analyze such a weak signal, long stretches of time need to be analyzed. Data folding provides a method to efficiently analyze these long time series. By exploiting an assumption of stationarity and the periodicity of the overlap function, entire LIGO observing runs worth of data can be averaged down to the size of one sidereal day. This will reduce computation time and storage by a factor of N_{day}, improving efficiency and making anisotropic stochastic analysis accessible to

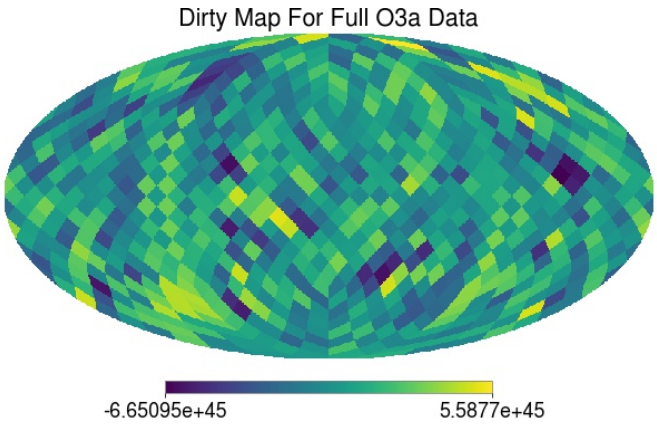

FIG. 16. Dirty map produced from the folded data from O3a.

anyone with a laptop.

We have shown that this algorithm functions with minimal loss of information on simulated data and can be applied to large volumes of real LIGO data. The code can handle large data cuts and can easily generalize to include more detectors.

An important next step involves the application of window functions to the data. These functions help reduce spectral line leakage, but lead to an effective loss of data. To prevent this data loss, we use 50% overlapping windows in SGWB analysis. These overlaps lead to some additional complications in the data folding algebra, which manifest as corrections to the X and Γ, but do not impede our ability to fold the data [4]. These corrections have yet to be implemented and therefore, the current algorithm only functions with non-overlapping windows.

VIII. ACKNOWLEDGMENTS

We would like to thank the National Science Foundation for sponsoring this project. We would also like to thank Alan Weinstein and LIGO lab for supervising, as well as Arianna Renzini and Colm Talbot for their mentorship. Finally, we'd like to thank Liting Xiao for providing the simulated stochastic dipole dataset.

[1] B. P. Abbott, R. Abbott, T. D. Abbott, M. R. Abernathy, F. Acernese, K. Ackley, C. Adams, T. Adams, P. Addesso, R. X. Adhikari, V. B. Adya, C. Affeldt, M. Agathos, K. Agatsuma, N. Aggarwal, O. D. Aguiar, L. Aiello, A. Ain, P. Ajith, B. Allen, A. Allocca, P. A. Altin, S. B. Anderson, W. G. Anderson, K. Arai, M. A. Arain, M. C. Araya, C. C. Arceneaux, J. S. Areeda, N. Arnaud, K. G. Arun, S. Ascenzi, G. Ashton, M. Ast, S. M. Aston, P. Astone, P. Aufmuth, C. Aulbert, S. Babak, P. Bacon, M. K. M. Bader, P. T. Baker, F. Baldaccini, G. Ballardin, S. W. Ballmer, J. C. Barayoga, S. E. Barclay, B. C. Barish, D. Barker, F. Barone, B. Barr, L. Barsotti, M. Barsuglia, D. Barta, J. Bartlett, M. A. Barton, I. Bartos, R. Bassiri, A. Basti, J. C. Batch, C. Baune, V. Bavigadda, M. Bazzan, B. Behnke, M. Bejger, C. Belczynski, A. S. Bell, C. J. Bell, B. K. Berger, J. Bergman, G. Bergmann, C. P. L. Berry, D. Bersanetti, A. Bertolini, J. Betzwieser, S. Bhagwat, R. Bhandare, I. A. Bilenko, G. Billingsley, J. Birch, R. Birney, O. Birnholtz, S. Biscans, A. Bisht, M. Bitossi, C. Biwer, M. A. Bizouard, J. K. Blackburn, C. D. Blair, D. G. Blair, R. M. Blair, S. Bloemen, O. Bock, T. P. Bodiya, M. Boer, G. Bogaert, C. Bogan, A. Bohe, P. Bojtos, C. Bond, F. Bondu, R. Bonnand, B. A. Boom, R. Bork, V. Boschi, S. Bose, Y. Bouffanais, A. Bozzi, C. Bradaschia, P. R. Brady, V. B. Braginsky, M. Branchesi, J. E. Brau, T. Briant, A. Brillet, M. Brinkmann, V. Brisson, P. Brockill, A. F. Brooks, D. A. Brown, D. D. Brown, N. M. Brown, C. C. Buchanan, A. Buikema, T. Bulik, H. J. Bulten, A. Buonanno, D. Buskulic, C. Buy, R. L. Byer, M. Cabero, L. Cadonati, G. Cagnoli, C. Cahillane, J. C. Bustillo, T. Callister, E. Calloni, J. B. Camp, K. C. Cannon, J. Cao, C. D. Capano, E. Capocasa, F. Carbognani, S. Caride, J. Casanueva Diaz, C. Casentini, S. Caudill, M. Cavaglià, F. Cavalier, R. Cavalieri, G. Cella, C. B. Cepeda, L. C. Baiardi, G. Cerretani, E. Cesarini, R. Chakraborty, T. Chalermsongsak, S. J. Chamberlin, M. Chan, S. Chao, P. Charlton, E. Chassande-Mottin, H. Y. Chen, Y. Chen, C. Cheng, A. Chincarini, A. Chiummo, H. S. Cho, M. Cho, J. H. Chow, N. Christensen, Q. Chu, S. Chua, S. Chung, G. Ciani, F. Clara, J. A. Clark, F. Cleva, E. Coccia, P. F. Cohadon, A. Colla, C. G. Collette, L. Cominsky, M. Constancio, A. Conte, L. Conti, D. Cook, T. R. Corbitt, N. Cornish, A. Corsi, S. Cortese, C. A. Costa, M. W. Coughlin, S. B. Coughlin, J. P. Coulon, S. T. Countryman, P. Couvares, E. E. Cowan, D. M. Coward, M. J. Cowart, D. C. Coyne, R. Coyne, K. Craig, J. D. E. Creighton, T. D. Creighton, J. Cripe, S. G. Crowder, A. M. Cruise, A. Cumming, L. Cunningham, E. Cuoco, T. Dal Canton, S. L. Danilishin, S. D'Antonio, K. Danzmann, N. S. Darman, C. F. Da Silva Costa, V. Dattilo, I. Dave, H. P. Daveloza, M. Davier, G. S. Davies, E. J. Daw, R. Day, S. De, D. DeBra, G. Debreczeni, J. Degallaix, M. De Laurentis, S. Deléglise, W. Del Pozzo, T. Denker, T. Dent, H. Dereli, V. Dergachev, R. T. DeRosa, R. De Rosa, R. DeSalvo, S. Dhurandhar, M. C. Díaz, L. Di Fiore, M. Di Giovanni, A. Di Lieto, S. Di Pace, I. Di Palma, A. Di Virgilio, G. Dojcinoski, V. Dolique, F. Donovan, K. L. Dooley, S. Doravari, R. Douglas, T. P. Downes, M. Drago, R. W. P. Drever, J. C. Driggers, Z. Du, M. Ducrot, S. E. Dwyer, T. B. Edo, M. C. Edwards, A. Effler, H. B. Eggenstein, P. Ehrens, J. Eichholz, S. S. Eikenberry, W. Engels, R. C. Essick, T. Etzel, M. Evans, T. M. Evans, R. Everett, M. Factourovich, V. Fafone, H. Fair, S. Fairhurst, X. Fan, Q. Fang, S. Farinon, B. Farr, W. M. Farr, M. Favata, M. Fays, H. Fehrmann, M. M. Fejer, D. Feldbaum, I. Ferrante, E. C. Ferreira, F. Ferrini, F. Fidecaro, L. S. Finn, I. Fiori, D. Fiorucci, R. P. Fisher,

R. Flaminio, M. Fletcher, H. Fong, J. D. Fournier, S. Franco, S. Frasca, F. Frasconi, M. Frede, Z. Frei, A. Freise, R. Frey, V. Frey, T. T. Fricke, P. Fritschel, V. V. Frolov, P. Fulda, M. Fyffe, H. A. G. Gabbard, J. R. Gair, L. Gammaitoni, S. G. Gaonkar, F. Garufi, A. Gatto, G. Gaur, N. Gehrels, G. Gemme, B. Gendre, E. Genin, A. Gennai, J. George, L. Gergely, V. Germain, A. Ghosh, A. Ghosh, S. Ghosh, J. A. Giaime, K. D. Giardina, A. Giazotto, K. Gill, A. Glaefke, J. R. Gleason, E. Goetz, R. Goetz, L. Gondan, G. González, J. M. G. Castro, A. Gopakumar, N. A. Gordon, M. L. Gorodetsky, S. E. Gossan, M. Gosselin, R. Gouaty, C. Graef, P. B. Graff, M. Granata, A. Grant, S. Gras, C. Gray, G. Greco, A. C. Green, R. J. S. Greenhalgh, P. Groot, H. Grote, S. Grunewald, G. M. Guidi, X. Guo, A. Gupta, M. K. Gupta, K. E. Gushwa, E. K. Gustafson, R. Gustafson, J. J. Hacker, B. R. Hall, E. D. Hall, G. Hammond, M. Haney, M. M. Hanke, J. Hanks, C. Hanna, M. D. Hannam, J. Hanson, T. Hardwick, J. Harms, G. M. Harry, I. W. Harry, M. J. Hart, M. T. Hartman, C. J. Haster, K. Haughian, J. Healy, J. Heefner, A. Heidmann, M. C. Heintze, G. Heinzel, H. Heitmann, P. Hello, G. Hemming, M. Hendry, I. S. Heng, J. Hennig, A. W. Heptonstall, M. Heurs, S. Hild, D. Hoak, K. A. Hodge, D. Hofman, S. E. Hollitt, K. Holt, D. E. Holz, P. Hopkins, D. J. Hosken, J. Hough, E. A. Houston, E. J. Howell, Y. M. Hu, S. Huang, E. A. Huerta, D. Huet, B. Hughey, S. Husa, S. H. Huttner, T. Huynh-Dinh, A. Idrisy, N. Indik, D. R. Ingram, R. Inta, H. N. Isa, J. M. Isac, M. Isi, G. Islas, T. Isogai, B. R. Iyer, K. Izumi, M. B. Jacobson, T. Jacqmin, H. Jang, K. Jani, P. Jaranowski, S. Jawahar, F. Jiménez-Forteza, W. W. Johnson, N. K. Johnson-McDaniel, D. I. Jones, R. Jones, R. J. G. Jonker, L. Ju, K. Haris, C. V. Kalaghatgi, V. Kalogera, S. Kandhasamy, G. Kang, J. B. Kanner, S. Karki, M. Kasprzack, E. Katsavounidis, W. Katzman, S. Kaufer, T. Kaur, K. Kawabe, F. Kawazoe, F. Kéfélian, M. S. Kehl, D. Keitel, D. B. Kelley, W. Kells, R. Kennedy, D. G. Keppel, J. S. Key, A. Khalaidovski, F. Y. Khalili, I. Khan, S. Khan, Z. Khan, E. A. Khazanov, N. Kijbunchoo, C. Kim, J. Kim, K. Kim, N.-G. Kim, N. Kim, Y. M. Kim, E. J. King, P. J. King, D. L. Kinzel, J. S. Kissel, L. Kleybolte, S. Klimenko, S. M. Koehlenbeck, K. Kokeyama, S. Koley, V. Kondrashov, A. Kontos, S. Koranda, M. Korobko, W. Z. Korth, I. Kowalska, D. B. Kozak, V. Kringel, B. Krishnan, A. Królak, C. Krueger, G. Kuehn, P. Kumar, R. Kumar, L. Kuo, A. Kutynia, P. Kwee, B. D. Lackey, M. Landry, J. Lange, B. Lantz, P. D. Lasky, A. Lazzarini, C. Lazzaro, P. Leaci, S. Leavey, E. O. Lebigot, C. H. Lee, H. K. Lee, H. M. Lee, K. Lee, A. Lenon, M. Leonardi, J. R. Leong, N. Leroy, N. Letendre, Y. Levin, B. M. Levine, T. G. F. Li, A. Libson, T. B. Littenberg, N. A. Lockerbie, J. Logue, A. L. Lombardi, L. T. London, J. E. Lord, M. Lorenzini, V. Loriette, M. Lormand, G. Losurdo, J. D. Lough, C. O. Lousto, G. Lovelace, H. Lück, A. P. Lundgren, J. Luo, R. Lynch, Y. Ma, T. MacDonald, B. Machenschalk, M. MacInnis, D. M. Macleod, F. Magaña-Sandoval, R. M. Magee, M. Mageswaran, E. Majorana, I. Maksimovic, V. Malvezzi, N. Man, I. Mandel, V. Mandic, V. Mangano, G. L. Mansell, M. Manske, M. Mantovani, F. Marchesoni, F. Marion, S. Márka, Z. Márka, A. S. Markosyan, E. Maros, F. Martelli, L. Martellini, I. W. Martin, R. M. Martin, D. V. Martynov, J. N. Marx, K. Mason, A. Masserot, T. J. Massinger, M. Masso-Reid, F. Matichard, L. Matone, N. Mavalvala, N. Mazumder, G. Mazzolo, R. McCarthy, D. E. McClelland, S. McCormick, S. C. McGuire, G. McIntyre, J. McIver, D. J. McManus, S. T. McWilliams, D. Meacher, G. D. Meadors, J. Meidam, A. Melatos, G. Mendell, D. Mendoza-Gandara, R. A. Mercer, E. Merilh, M. Merzougui, S. Meshkov, C. Messenger, C. Messick, P. M. Meyers, F. Mezzani, H. Miao, C. Michel, H. Middleton, E. E. Mikhailov, L. Milano, J. Miller, M. Millhouse, Y. Minenkov, J. Ming, S. Mirshekari, C. Mishra, S. Mitra, V. P. Mitrofanov, G. Mitselmakher, R. Mittleman, A. Moggi, M. Mohan, S. R. P. Mohapatra, M. Montani, B. C. Moore, C. J. Moore, D. Moraru, G. Moreno, S. R. Morriss, K. Mossavi, B. Mours, C. M. Mow-Lowry, C. L. Mueller, G. Mueller, A. W. Muir, A. Mukherjee, D. Mukherjee, S. Mukherjee, N. Mukund, A. Mullavey, J. Munch, D. J. Murphy, P. G. Murray, A. Mytidis, I. Nardecchia, L. Naticchioni, R. K. Nayak, V. Necula, K. Nedkova, G. Nelemans, M. Neri, A. Neunzert, G. Newton, T. T. Nguyen, A. B. Nielsen, S. Nissanke, A. Nitz, F. Nocera, D. Nolting, M. E. N. Normandin, L. K. Nuttall, J. Oberling, E. Ochsner, J. O'Dell, E. Oelker, G. H. Ogin, J. J. Oh, S. H. Oh, F. Ohme, M. Oliver, P. Oppermann, R. J. Oram, B. O'Reilly, R. O'Shaughnessy, C. D. Ott, D. J. Ottaway, R. S. Ottens, H. Overmier, B. J. Owen, A. Pai, S. A. Pai, J. R. Palamos, O. Palashov, C. Palomba, A. Pal-Singh, H. Pan, Y. Pan, C. Pankow, F. Pannarale, B. C. Pant, F. Paoletti, A. Paoli, M. A. Papa, H. R. Paris, W. Parker, D. Pascucci, A. Pasqualetti, R. Passaquieti, D. Passuello, B. Patricelli, Z. Patrick, B. L. Pearlstone, M. Pedraza, R. Pedurand, L. Pekowsky, A. Pele, S. Penn, A. Perreca, H. P. Pfeiffer, M. Phelps, O. Piccinni, M. Pichot, M. Pickenpack, F. Piergiovanni, V. Pierro, G. Pillant, L. Pinard, I. M. Pinto, M. Pitkin, J. H. Poeld, R. Poggiani, P. Popolizio, A. Post, J. Powell, J. Prasad, V. Predoi, S. S. Premachandra, T. Prestegard, L. R. Price, M. Prijatelj, M. Principe, S. Privitera, R. Prix, G. A. Prodi, L. Prokhorov, O. Puncken, M. Punturo, P. Puppo, M. Pürrer, H. Qi, J. Qin, V. Quetschke, E. A. Quintero, R. Quitzow-James, F. J. Raab, D. S. Rabeling, H. Radkins, P. Raffai, S. Raja, M. Rakhmanov, C. R. Ramet, P. Rapagnani, V. Raymond, M. Razzano, V. Re, J. Read, C. M. Reed, T. Regimbau, L. Rei, S. Reid, D. H. Reitze, H. Rew, S. D. Reyes, F. Ricci, K. Riles, N. A. Robertson, R. Robie, F. Robinet, A. Rocchi, L. Rolland, J. G. Rollins, V. J. Roma, J. D. Romano, R. Romano, G. Romanov, J. H. Romie, D. Rosińska, S. Rowan, A. Rüdiger, P. Ruggi, K. Ryan, S. Sachdev, T. Sadecki, L. Sadeghian, L. Salconi, M. Saleem, F. Salemi, A. Samajdar, L. Sammut, L. M. Sampson, E. J. Sanchez, V. Sandberg, B. Sandeen, G. H. Sanders, J. R. Sanders, B. Sassolas, B. S. Sathyaprakash, P. R. Saulson, O. Sauter, R. L. Savage, A. Sawadsky, P. Schale, R. Schilling, J. Schmidt, P. Schmidt, R. Schnabel, R. M. S. Schofield, A. Schönbeck, E. Schreiber, D. Schuette, B. F. Schutz, J. Scott, S. M. Scott, D. Sellers, A. S. Sengupta, D. Sentenac, V. Sequino, A. Sergeev, G. Serna, Y. Setyawati, A. Sevigny, D. A. Shaddock, T. Shaffer, S. Shah, M. S. Shahriar, M. Shaltev, Z. Shao, B. Shapiro, P. Shawhan, A. Sheperd, D. H. Shoemaker, D. M. Shoemaker, K. Siellez, X. Siemens, D. Sigg, A. D. Silva, D. Simakov, A. Singer, L. P. Singer, A. Singh, R. Singh, A. Sing-

hal, A. M. Sintes, B. J. J. Slagmolen, J. R. Smith, M. R. Smith, N. D. Smith, R. J. E. Smith, E. J. Son, B. Sorazu, F. Sorrentino, T. Souradeep, A. K. Srivastava, A. Staley, M. Steinke, J. Steinlechner, S. Steinlechner, D. Steinmeyer, B. C. Stephens, S. P. Stevenson, R. Stone, K. A. Strain, N. Straniero, G. Stratta, N. A. Strauss, S. Strigin, R. Sturani, A. L. Stuver, T. Z. Summerscales, L. Sun, P. J. Sutton, B. L. Swinkels, M. J. Szczepańczyk, M. Tacca, D. Talukder, D. B. Tanner, M. Tápai, S. P. Tarabrin, A. Taracchini, R. Taylor, T. Theeg, M. P. Thirugnanasambandam, E. G. Thomas, M. Thomas, P. Thomas, K. A. Thorne, K. S. Thorne, E. Thrane, S. Tiwari, V. Tiwari, K. V. Tokmakov, C. Tomlinson, M. Tonelli, C. V. Torres, C. I. Torrie, D. Töyrä, F. Travasso, G. Traylor, D. Trifirò, M. C. Tringali, L. Trozzo, M. Tse, M. Turconi, D. Tuyenbayev, D. Ugolini, C. S. Unnikrishnan, A. L. Urban, S. A. Usman, H. Vahlbruch, G. Vajente, G. Valdes, M. Vallisneri, N. van Bakel, M. van Beuzekom, J. F. J. van den Brand, C. Van Den Broeck, D. C. Vander-Hyde, L. van der Schaaf, J. V. van Heijningen, A. A. van Veggel, M. Vardaro, S. Vass, M. Vasúth, R. Vaulin, A. Vecchio, G. Vedovato, J. Veitch, P. J. Veitch, K. Venkateswara, D. Verkindt, F. Vetrano, A. Viceré, S. Vinciguerra, D. J. Vine, J. Y. Vinet, S. Vitale, T. Vo, H. Vocca, C. Vorvick, D. Voss, W. D. Vousden, S. P. Vyatchanin, A. R. Wade, L. E. Wade, M. Wade, S. J. Waldman, M. Walker, L. Wallace, S. Walsh, G. Wang, H. Wang, M. Wang, X. Wang, Y. Wang, H. Ward, R. L. Ward, J. Warner, M. Was, B. Weaver, L. W. Wei, M. Weinert, A. J. Weinstein, R. Weiss, T. Welborn, L. Wen, P. Weßels, T. Westphal, K. Wette, J. T. Whelan, S. E. Whitcomb, D. J. White, B. F. Whiting, K. Wiesner, C. Wilkinson, P. A. Willems, L. Williams, R. D. Williams, A. R. Williamson, J. L. Willis, B. Willke, M. H. Wimmer, L. Winkelmann, W. Winkler, C. C. Wipf, A. G. Wiseman, H. Wittel, G. Woan, J. Worden, J. L. Wright, G. Wu, J. Yablon, I. Yakushin, W. Yam, H. Yamamoto, C. C. Yancey, M. J. Yap, H. Yu, M. Yvert, A. ZadroŻny, L. Zangrando, M. Zanolin, J. P. Zendri, M. Zevin, F. Zhang, L. Zhang, M. Zhang, Y. Zhang, C. Zhao, M. Zhou, Z. Zhou, X. J. Zhu, M. E. Zucker, S. E. Zuraw, J. Zweizig, LIGO Scientific Collaboration, and Virgo Collaboration, Observation of Gravitational Waves from a Binary Black Hole Merger, Phys. Rev. Lett. **116**, 061102 (2016), arXiv:1602.03837 [gr-qc].

[2] A. H. Nitz, C. D. Capano, S. Kumar, Y.-F. Wang, S. Kastha, M. Schäfer, R. Dhurkunde, and M. Cabero, 3-OGC: Catalog of gravitational waves from compact-binary mergers, arXiv e-prints , arXiv:2105.09151 (2021), arXiv:2105.09151 [astro-ph.HE].

[3] J. Romano and N. Cornish, Detection methods for stochastic gravitational-wave backgrounds: A unified treatment, Living Reviews in Relativity **20** (2017).

[4] A. Ain, P. Dalvi, and S. Mitra, Fast gravitational wave radiometry using data folding, Phys. Rev. D **92**, 022003 (2015).

[5] A. Renzini, *Mapping the gravitational-wave background*, Ph.D. thesis, Imperial College London (2020).

[6] Planck Collaboration, N. Aghanim, Y. Akrami, F. Arroja, M. Ashdown, J. Aumont, C. Baccigalupi, M. Ballardini, A. J. Banday, R. B. Barreiro, N. Bartolo, S. Basak, R. Battye, K. Benabed, J. P. Bernard, M. Bersanelli, P. Bielewicz, J. J. Bock, J. R. Bond, J. Borrill, F. R. Bouchet, F. Boulanger, M. Bucher, C. Burigana, R. C. Butler, E. Calabrese, J. F. Cardoso, J. Carron, B. Casaponsa, A. Challinor, H. C. Chiang, L. P. L. Colombo, C. Combet, D. Contreras, B. P. Crill, F. Cuttaia, P. de Bernardis, G. de Zotti, J. Delabrouille, J. M. Delouis, F. X. Désert, E. Di Valentino, C. Dickinson, J. M. Diego, S. Donzelli, O. Doré, M. Douspis, A. Ducout, X. Dupac, G. Efstathiou, F. Elsner, T. A. Enßlin, H. K. Eriksen, E. Falgarone, Y. Fantaye, J. Fergusson, R. Fernandez-Cobos, F. Finelli, F. Forastieri, M. Frailis, E. Franceschi, A. Frolov, S. Galeotta, S. Galli, K. Ganga, R. T. Génova-Santos, M. Gerbino, T. Ghosh, J. González-Nuevo, K. M. Górski, S. Gratton, A. Gruppuso, J. E. Gudmundsson, J. Hamann, W. Handley, F. K. Hansen, G. Helou, D. Herranz, S. R. Hildebrandt, E. Hivon, Z. Huang, A. H. Jaffe, W. C. Jones, A. Karakci, E. Keihänen, R. Keskitalo, K. Kiiveri, J. Kim, T. S. Kisner, L. Knox, N. Krachmalnicoff, M. Kunz, H. Kurki-Suonio, G. Lagache, J. M. Lamarre, M. Langer, A. Lasenby, M. Lattanzi, C. R. Lawrence, M. Le Jeune, J. P. Leahy, J. Lesgourgues, F. Levrier, A. Lewis, M. Liguori, P. B. Lilje, M. Lilley, V. Lindholm, M. López-Caniego, P. M. Lubin, Y. Z. Ma, J. F. Macías-Pérez, G. Maggio, D. Maino, N. Mandolesi, A. Mangilli, A. Marcos-Caballero, M. Maris, P. G. Martin, M. Martinelli, E. Martínez-González, S. Matarrese, N. Mauri, J. D. McEwen, P. D. Meerburg, P. R. Meinhold, A. Melchiorri, A. Mennella, M. Migliaccio, M. Millea, S. Mitra, M. A. Miville-Deschênes, D. Molinari, A. Moneti, L. Montier, G. Morgante, A. Moss, S. Mottet, M. Münchmeyer, P. Natoli, H. U. Nørgaard-Nielsen, C. A. Oxborrow, L. Pagano, D. Paoletti, B. Partridge, G. Patanchon, T. J. Pearson, M. Peel, H. V. Peiris, F. Perrotta, V. Pettorino, F. Piacentini, L. Polastri, G. Polenta, J. L. Puget, J. P. Rachen, M. Reinecke, M. Remazeilles, C. Renault, A. Renzi, G. Rocha, C. Rosset, G. Roudier, J. A. Rubiño-Martín, B. Ruiz-Granados, L. Salvati, M. Sandri, M. Savelainen, D. Scott, E. P. S. Shellard, M. Shiraishi, C. Sirignano, G. Sirri, L. D. Spencer, R. Sunyaev, A. S. Suur-Uski, J. A. Tauber, D. Tavagnacco, M. Tenti, L. Terenzi, L. Toffolatti, M. Tomasi, T. Trombetti, J. Valiviita, B. Van Tent, L. Vibert, P. Vielva, F. Villa, N. Vittorio, B. D. Wandelt, I. K. Wehus, M. White, S. D. M. White, A. Zacchei, and A. Zonca, Planck 2018 results. I. Overview and the cosmological legacy of Planck, aap **641**, A1 (2020), arXiv:1807.06205 [astro-ph.CO].

[7] J. Ellis, M. Fairbairn, M. Lewicki, V. Vaskonen, and A. Wickens, Detecting circular polarisation in the stochastic gravitational-wave background from a first-order cosmological phase transition, Journal of Cosmology and Astroparticle Physics **2020** (10), 032–032.

[8] T. L. S. Collaboration, T. V. Collaboration, *et al.*, Upper limits on the isotropic gravitational-wave background from advanced ligo's and advanced virgo's third observing run (2021).

[9] H. Grote and D. H. Reitze, First-Generation Interferometric Gravitational-Wave Detectors, in *46th Rencontres de Moriond on Gravitational Waves and Experimental Gravity* (Moriond, Paris, France, 2011).

[10] B. F. Schutz, *A First Course in General Relativity* (Cambridge University Press, Cambridge, 2011).

[11] A. Buikema, C. Cahillane, G. L. Mansell, C. D. Blair, R. Abbott, C. Adams, R. X. Adhikari, A. Ananyeva, S. Appert, K. Arai, J. S. Areeda, Y. Asali, S. M. As-

ton, C. Austin, A. M. Baer, M. Ball, S. W. Ballmer, S. Banagiri, D. Barker, L. Barsotti, J. Bartlett, B. K. Berger, J. Betzwieser, D. Bhattacharjee, G. Billingsley, S. Biscans, R. M. Blair, N. Bode, P. Booker, R. Bork, A. Bramley, A. F. Brooks, D. D. Brown, K. C. Cannon, X. Chen, A. A. Ciobanu, F. Clara, S. J. Cooper, K. R. Corley, S. T. Countryman, P. B. Covas, D. C. Coyne, L. E. H. Datrier, D. Davis, C. Di Fronzo, K. L. Dooley, J. C. Driggers, P. Dupej, S. E. Dwyer, A. Effler, T. Etzel, M. Evans, T. M. Evans, J. Feicht, A. Fernandez-Galiana, P. Fritschel, V. V. Frolov, P. Fulda, M. Fyffe, J. A. Giaime, K. D. Giardina, P. Godwin, E. Goetz, S. Gras, C. Gray, R. Gray, A. C. Green, E. K. Gustafson, R. Gustafson, J. Hanks, J. Hanson, T. Hardwick, R. K. Hasskew, M. C. Heintze, A. F. Helmling-Cornell, N. A. Holland, J. D. Jones, S. Kandhasamy, S. Karki, M. Kasprzack, K. Kawabe, N. Kijbunchoo, P. J. King, J. S. Kissel, R. Kumar, M. Landry, B. B. Lane, B. Lantz, M. Laxen, Y. K. Lecoeuche, J. Leviton, J. Liu, M. Lormand, A. P. Lundgren, R. Macas, M. MacInnis, D. M. Macleod, S. Márka, Z. Márka, D. V. Martynov, K. Mason, T. J. Massinger, F. Matichard, N. Mavalvala, R. McCarthy, D. E. McClelland, S. McCormick, L. McCuller, J. McIver, T. McRae, G. Mendell, K. Merfeld, E. L. Merilh, F. Meylahn, T. Mistry, R. Mittleman, G. Moreno, C. M. Mow-Lowry, S. Mozzon, A. Mullavey, T. J. N. Nelson, P. Nguyen, L. K. Nuttall, J. Oberling, R. J. Oram, B. O'Reilly, C. Osthelder, D. J. Ottaway, H. Overmier, J. R. Palamos, W. Parker, E. Payne, A. Pele, R. Penhorwood, C. J. Perez, M. Pirello, H. Radkins, K. E. Ramirez, J. W. Richardson, K. Riles, N. A. Robertson, J. G. Rollins, C. L. Romel, J. H. Romie, M. P. Ross, K. Ryan, T. Sadecki, E. J. Sanchez, L. E. Sanchez, T. R. Saravanan, R. L. Savage, D. Schaetzl, R. Schnabel, R. M. S. Schofield, E. Schwartz, D. Sellers, T. Shaffer, D. Sigg, B. J. J. Slagmolen, J. R. Smith, S. Soni, B. Sorazu, A. P. Spencer, K. A. Strain, L. Sun, M. J. Szczepańczyk, M. Thomas, P. Thomas, K. A. Thorne, K. Toland, C. I. Torrie, G. Traylor, M. Tse, A. L. Urban, G. Vajente, G. Valdes, D. C. Vander-Hyde, P. J. Veitch, K. Venkateswara, G. Venugopalan, A. D. Viets, T. Vo, C. Vorvick, M. Wade, R. L. Ward, J. Warner, B. Weaver, R. Weiss, C. Whittle, B. Willke, C. C. Wipf, L. Xiao, H. Yamamoto, H. Yu, H. Yu, L. Zhang, M. E. Zucker, and J. Zweizig, Sensitivity and performance of the advanced ligo detectors in the third observing run, Phys. Rev. D **102**, 062003 (2020).

[12] B. Abbott *et al.* (The LIGO Scientific Collaboration and the Virgo Collaboration), Directional limits on persistent gravitational waves using data from advanced ligo's first two observing runs, Phys. Rev. D **100**, 062001 (2019).

[13] L. S. Finn, S. L. Larson, and J. D. Romano, Detecting a stochastic gravitational-wave background: The overlap reduction function, Phys. Rev. D **79**, 062003 (2009).

[14] P. B. Covas, A. Effler, E. Goetz, P. M. Meyers, A. Neunzert, M. Oliver, B. L. Pearlstone, V. J. Roma, R. M. S. Schofield, V. B. Adya, P. Astone, S. Biscoveanu, T. A. Callister, N. Christensen, A. Colla, E. Coughlin, M. W. Coughlin, S. G. Crowder, S. E. Dwyer, H. B. Eggenstein, S. Hourihane, S. Kandhasamy, W. Liu, A. P. Lundgren, A. Matas, R. McCarthy, J. McIver, G. Mendell, R. Ormiston, C. Palomba, M. A. Papa, O. J. Piccinni, K. Rao, K. Riles, L. Sammut, S. Schlassa, D. Sigg, N. Strauss, D. Tao, K. A. Thorne, E. Thrane, S. Trembath-Reichert, B. P. Abbott, R. Abbott, T. D. Abbott, C. Adams, R. X. Adhikari, A. Ananyeva, S. Appert, K. Arai, S. M. Aston, C. Austin, S. W. Ballmer, D. Barker, B. Barr, L. Barsotti, J. Bartlett, I. Bartos, J. C. Batch, M. Bejger, A. S. Bell, J. Betzwieser, G. Billingsley, J. Birch, S. Biscans, C. Biwer, C. D. Blair, R. M. Blair, R. Bork, A. F. Brooks, H. Cao, G. Ciani, F. Clara, P. Clearwater, S. J. Cooper, P. Corban, S. T. Countryman, M. J. Cowart, D. C. Coyne, A. Cumming, L. Cunningham, K. Danzmann, C. F. D. S. Costa, E. J. Daw, D. DeBra, R. T. DeRosa, R. DeSalvo, K. L. Dooley, S. Doravari, J. C. Driggers, T. B. Edo, T. Etzel, M. Evans, T. M. Evans, M. Factourovich, H. Fair, A. F. Galiana, E. C. Ferreira, R. P. Fisher, H. Fong, R. Frey, P. Fritschel, V. V. Frolov, P. Fulda, M. Fyffe, B. Gateley, J. A. Giaime, K. D. Giardina, R. Goetz, B. Goncharov, S. Gras, C. Gray, H. Grote, K. E. Gushwa, E. K. Gustafson, R. Gustafson, E. D. Hall, G. Hammond, J. Hanks, J. Hanson, T. Hardwick, G. M. Harry, M. C. Heintze, A. W. Heptonstall, J. Hough, R. Inta, K. Izumi, R. Jones, S. Karki, M. Kasprzack, S. Kaufer, K. Kawabe, R. Kennedy, N. Kijbunchoo, W. Kim, E. J. King, P. J. King, J. S. Kissel, W. Z. Korth, G. Kuehn, M. Landry, B. Lantz, M. Laxen, J. Liu, N. A. Lockerbie, M. Lormand, M. MacInnis, D. M. Macleod, S. Márka, Z. Márka, A. S. Markosyan, E. Maros, P. Marsh, I. W. Martin, D. V. Martynov, K. Mason, T. J. Massinger, F. Matichard, N. Mavalvala, D. E. McClelland, S. McCormick, L. McCuller, G. McIntyre, T. McRae, E. L. Merilh, J. Miller, R. Mittleman, G. Mo, K. Mogushi, D. Moraru, G. Moreno, G. Mueller, N. Mukund, A. Mullavey, J. Munch, T. J. N. Nelson, P. Nguyen, L. K. Nuttall, J. Oberling, O. Oktavia, P. Oppermann, R. J. Oram, B. O'Reilly, D. J. Ottaway, H. Overmier, J. R. Palamos, W. Parker, A. Pele, S. Penn, C. J. Perez, M. Phelps, V. Pierro, I. Pinto, M. Principe, L. G. Prokhorov, O. Puncken, V. Quetschke, E. A. Quintero, H. Radkins, P. Raffai, K. E. Ramirez, S. Reid, D. H. Reitze, N. A. Robertson, J. G. Rollins, C. L. Romel, J. H. Romie, M. P. Ross, S. Rowan, K. Ryan, T. Sadecki, E. J. Sanchez, L. E. Sanchez, V. Sandberg, R. L. Savage, D. Sellers, D. A. Shaddock, T. J. Shaffer, B. Shapiro, D. H. Shoemaker, B. J. J. Slagmolen, B. Smith, J. R. Smith, B. Sorazu, A. P. Spencer, A. Staley, K. A. Strain, L. Sun, D. B. Tanner, J. D. Tasson, R. Taylor, M. Thomas, P. Thomas, K. Toland, C. I. Torrie, G. Traylor, M. Tse, D. Tuyenbayev, G. Vajente, G. Valdes, A. A. van Veggel, A. Vecchio, P. J. Veitch, K. Venkateswara, T. Vo, C. Vorvick, M. Wade, M. Walker, R. L. Ward, J. Warner, B. Weaver, R. Weiss, P. Weßels, B. Willke, C. C. Wipf, J. Wofford, J. Worden, H. Yamamoto, C. C. Yancey, H. Yu, H. Yu, L. Zhang, S. Zhu, M. E. Zucker, J. Zweizig, and LSC Instrument Authors, Identification and mitigation of narrow spectral artifacts that degrade searches for persistent gravitational waves in the first two observing runs of Advanced LIGO, Phys. Rev. D **97**, 082002 (2018), arXiv:1801.07204 [astro-ph.IM].